Momentum-space solution of exciton excited states and heavy-hole–light-hole mixing in quantum wells

Calvin Yi-Ping Chao* and Shun Lien Chuang
Department of Electrical and Computer Engineering, University of Illinois, 1406 West Green Street, Urbana, Illinois 61801
(Received 2 November 1992)

A full valence-band mixing model for excitons in quantum wells is presented. The exciton equation is solved in momentum space using the modified Gaussian quadrature method, taking into account the angular dependence of the excitons. The theory accounts for the mixing of the ground state of the light-hole exciton and the excited states of the heavy-hole exciton at low temperatures reported previously by Viña *et al.* [Phys. Rev. Lett. **58**, 832 (1987)]. Our calculations reproduce correctly the resonant field, the minimum energy split at the resonant field, and the fine structure of the competing $2s$ and $2p$ states resolved in the experimental data. For the s-states-dominated spectra, the full model can be simplified to include only s-states coupling. We show that the numerical results based on the simplified model match very well the polarization-dependent room-temperature exciton absorption spectra of Miller *et al.* [IEEE J. Quantum Electron. **QE-22**, 1816 (1986)].

I. INTRODUCTION

The continuous improvement in the crystal-growth technology in the last quarter of the century has allowed scientists to grow a wide range of semiconductor materials, literally speaking, atomic layer by atomic layer. With this capability, the optoelectronic properties of multilayered structures can be manipulated such that a few new physical phenomena have been discovered and a variety of new devices has been engineered. A recent survey on the physics and applications of the semiconductor heterostructures can be found, for example, in the books by Bastard,[1] Weisbuch and Vinter,[2] Ref. 3, and the references therein.

The first step towards understanding the optoelectronic properties of a quantum-well device is to calculate the quantum-confined electron and hole states in the well. For most semiconductors, the conduction band is well approximated by a parabolic-band model, which characterizes the electron motion by a single, isotropic effective mass. The nonparabolicity of the conduction band is usually not important when the energy of interest is less than, for instance, 100 meV above the conduction-band edge. On the other hand, the valence bands of most direct-band-gap semiconductors are more complicated; the heavy-hole and the light-hole bands are degenerate at $k = 0$ and are strongly coupled at $k \neq 0$. In quantum wells, this coupling leads to a highly nonparabolic subband structure. Experimentally, the observation of "forbidden" excitonic transitions[4,5] and the mixing of heavy-hole and light-hole excitons[6] have provided direct and strong evidence of the valence-band mixing.

The calculations of the valence-subband structures of quantum wells are usually based on the Luttinger-Kohn effective-mass theory,[7,8] which describes the valence band by a 6×6 effective-mass tensor. Various effects such as the electric field and strain can be easily included in the Luttinger-Kohn Hamiltonian.

Excitonic effects play important roles on the optical properties of direct-band-gap semiconductor quantum wells near the band edge.[9,10] The advance in technology has allowed routine observation of excitonic transitions between different conduction and valence subbands. In addition to the ground state, the excited states of quantum-well excitons have also been detected by various techniques.[11–15]

A number of exciton theories and models have been developed by researchers[16–22] to interpret experimental data. The exciton binding energies and oscillator strengths are usually calculated by variational methods in either real space or momentum space. But the variational method becomes less practical when one tries to incorporate all together the exciton continuum states, the mixing among hole subbands, and the angular dependence of the exciton wave functions, because a large number of basis functions would be needed.

On the other hand, it is known that the quadrature method can be used to solve an integral equation accurately and efficiently. For example, a modified Gaussian quadrature method has been applied to investigate the Fano resonance between the exciton discrete states and continuum states,[20] to calculate the exciton Green's function,[23] and to study the anticrossing between the direct and indirect excitons in coupled quantum wells.[24] The accuracy of the quadrature method has been checked by solving a pure two-dimensional exciton problem with known exact solutions.[25] Similar numerical methods by discretizing the exciton eigenvalue equation in $\boldsymbol{k}$ space without the variational approach have also been used to study quantum-well excitons.[19,21]

The purpose of this paper is to extend the modified Gaussian quadrature method to solve the exciton effective-mass equation in momentum space, properly taking into account the mixing between the heavy-hole

0163-1829/93/48(11)/8210(12)/$06.00

and light-hole subbands and the angular dependence of the exciton states. In Sec. II, a general exciton theory based on the band-mixing model is presented, followed by discussions on the angular-momentum quantum number and the axial approximation. In Sec. III we first show that a simplified model can be used to match the experimental data predominated by s-state excitons, such as the room-temperature exciton absorption spectra of Miller, Weiner, and Chemla.[10] Then, the full band-mixing model is applied to explain the low-temperature photoluminescence excitation (PLE) spectra of Viña *et al.*[6] It is shown that the model is able to not only explain the anticrossing between the heavy-hole and light-hole excitons, but also to account for the fine structure of the exciton $2s$ and $2p$ excited states. The calculated exciton spectra and energies as functions of fields are compared to experimental data. Finally, conclusions are given in Sec. IV and details of the numerical method are given in the Appendix.

II. EXCITON THEORY WITH VALENCE-BAND MIXING

A. Full band-mixing model

Within the framework of the Luttinger-Kohn effective-mass theory[7,8] and the envelope-function scheme,[1] the exciton Hamiltonian can be written as

$$\mathcal{H}_{\nu\nu'} = H^e\,\delta_{\nu\nu'} + H^h_{\nu\nu'} + V_{\rm Coul}\,\delta_{\nu\nu'} , \tag{1}$$

$$V_{\rm Coul} = -\frac{e^2}{4\pi\epsilon_0\epsilon}\frac{1}{|\boldsymbol{r}_e - \boldsymbol{r}_h|} , \tag{2}$$

$$H^e = E_c(-i\nabla) + V_e(z_e) - eFz_e , \tag{3}$$

$$H^h_{\nu\nu'} = H^{\rm LK}_{\nu\nu'} + V_h(z_h) + eFz_h , \tag{4}$$

where V_e, V_h, and $V_{\rm Coul}$ are the electron quantum-well potential, the hole quantum-well potential, and the Coulomb potential, respectively. The electron kinetic-energy operator $E_c(-i\nabla)$ is obtained directly from the conduction-band dispersion relation $E_c(\boldsymbol{k})$, and the hole kinetic-energy operator is taken as the Luttinger-Kohn effective-mass tensor $H^{\rm LK}_{\nu\nu'}$. For the material system such as GaAs/$Al_xGa_{1-x}As$, the spin-orbit spilt-off band can be safely ignored;[26] therefore, the 4×4 matrix formulation is adequate and the hole spin index ν runs from $-\frac{3}{2}$ to $\frac{3}{2}$.

The energies and envelope functions of the conduction and valence subbands are obtained by solving

$$H^e f_{n\sigma}(\boldsymbol{k},\boldsymbol{r}_e) = E^e_n(k) f_{n\sigma}(\boldsymbol{k},\boldsymbol{r}_e) \tag{5}$$

and

$$\sum_{\nu'} H^h_{\nu\nu'}\, g_{m\nu'}(\boldsymbol{k},\boldsymbol{r}_h) = E^h_m(\boldsymbol{k}) g_{m\nu}(\boldsymbol{k},\boldsymbol{r}_h) , \tag{6}$$

respectively, where σ (equal to $\frac{1}{2}$ or $-\frac{1}{2}$) is the electron spin index. The envelope functions are normalized in the following way:

$$f_{n\sigma}(\boldsymbol{k},\boldsymbol{r}_e) = (2\pi)^{-1} f_{n\sigma}(\boldsymbol{k},z_e)\,\exp(i\boldsymbol{k}\cdot\boldsymbol{\rho}_e) , \tag{7}$$

$$g_{m\nu}(\boldsymbol{k},\boldsymbol{r}_h) = (2\pi)^{-1} g_{m\nu}(\boldsymbol{k},z_h)\,\exp(i\boldsymbol{k}\cdot\boldsymbol{\rho}_h) , \tag{8}$$

$$\int d^3\boldsymbol{r}_e f^*_{n\sigma}(\boldsymbol{k},\boldsymbol{r}_e) f_{n'\sigma}(\boldsymbol{k}',\boldsymbol{r}_e) = \delta_{nn'}\,\delta(\boldsymbol{k}-\boldsymbol{k}') , \tag{9}$$

$$\int d^3\boldsymbol{r}_h \sum_\nu g^*_{m\nu}(\boldsymbol{k},\boldsymbol{r}_h) g_{m'\nu}(\boldsymbol{k}',\boldsymbol{r}_h) = \delta_{mm'}\,\delta(\boldsymbol{k}-\boldsymbol{k}') , \tag{10}$$

$$\int dz_e f^*_{n\sigma}(\boldsymbol{k},z_e) f_{n'\sigma}(\boldsymbol{k},z_e) = \delta_{nn'} , \tag{11}$$

$$\int dz_h \sum_\nu g^*_{m\nu}(\boldsymbol{k},z_h) g_{m'\nu}(\boldsymbol{k},z_h) = \delta_{mm'} , \tag{12}$$

where the n and m are the labels for the conduction and valence subbands. The vectors $\boldsymbol{k}$ and $\boldsymbol{\rho}$ refer to two-dimensional vectors in the x-y plane.

One important fact often overlooked is that the electron wave function depends on the azimuthal angle θ of the vector $\boldsymbol{k}$, even though the the electron Hamiltonian H^e depends only on the magnitude of $\boldsymbol{k}$ in the current model. The implicit θ dependence,

$$f_{n\sigma}(\boldsymbol{k},z_e) = f_n(k,z_e)\,e^{-i\sigma\theta} , \tag{13}$$

becomes clear when the coupling between the conduction band and the valence band is taken into account, as in Kane's model.[27–29] The θ dependence of the valence-band energies and wave functions is more complicated and will be discussed later.

The exciton wave function is a four-component spinor satisfying the coupled differential equation in coordinate space

$$\sum_{\nu'} \mathcal{H}_{\nu\nu'}\,\Psi^X_{\nu'}(\boldsymbol{r}_e,\boldsymbol{r}_h) = E_X\,\Psi^X_\nu(\boldsymbol{r}_e,\boldsymbol{r}_h) , \tag{14}$$

where X labels different exciton states, for example, $X = 1s, 2s, 2p$, and so forth. Similarly to the momentum-space formulation in the parabolic-band model,[23] the exciton wave function can be expanded as ($\boldsymbol{\rho} = \boldsymbol{\rho}_e - \boldsymbol{\rho}_h$)

$$\Psi^X_\nu(\boldsymbol{\rho},z_e,z_h) = \sum_{n,m}\int \frac{d^2\boldsymbol{k}}{(2\pi)^2}\,\phi^X_{nm}(\boldsymbol{k}) f_{n\sigma}(\boldsymbol{k},z_e) \times g_{m\nu}(\boldsymbol{k},z_h)\exp(i\boldsymbol{k}\cdot\boldsymbol{\rho}) , \tag{15}$$

and normalized according to

$$\int d^2\boldsymbol{\rho}\int dz_e\int dz_h \sum_\nu \Psi^{X*}_\nu(\boldsymbol{\rho},z_e,z_h)\,\Psi^{X'}_\nu(\boldsymbol{\rho},z_e,z_h) = \sum_{n,m}\int\frac{d^2\boldsymbol{k}}{(2\pi)^2}\,\phi^{X*}_{nm}(\boldsymbol{k})\,\phi^{X'}_{nm}(\boldsymbol{k}) = \delta_{XX'} . \tag{16}$$

By multiplying both sides of Eq. (14) by $f^*_{n\sigma}(\boldsymbol{k},z_e) g^*_{m\nu}(\boldsymbol{k},z_h)\exp(-i\boldsymbol{k}\cdot\boldsymbol{\rho})$, summing over ν, and

integrating them over z_e, z_h, and $\boldsymbol{\rho}$, the exciton equation in $\boldsymbol{k}$ space becomes

$$T_{nm}(\boldsymbol{k})\phi^X_{nm}(\boldsymbol{k}) + \sum_{n',m'} \int \frac{d^2\boldsymbol{k}'}{(2\pi)^2} V_{nmn'm'}(\boldsymbol{k},\boldsymbol{k}')\phi^X_{n'm'}(\boldsymbol{k}') = E_X \phi^X_{nm}(\boldsymbol{k}) , \quad (17)$$

where

$$T_{nm}(\boldsymbol{k}) = E^e_n(k) + E^h_m(\boldsymbol{k}) , \quad (18)$$

and

$$V_{nmn'm'}(\boldsymbol{k},\boldsymbol{k}') = -\frac{e^2}{2\epsilon_0\epsilon\,|\boldsymbol{k}-\boldsymbol{k}'|} \int dz_e \int dz_h \, \exp(-|\boldsymbol{k}-\boldsymbol{k}'| \times |z_e - z_h|) \times \sum_\nu f^*_{n\sigma}(\boldsymbol{k},z_e) f_{n'\sigma}(\boldsymbol{k}',z_e) g^*_{m\nu}(\boldsymbol{k},z_h) g_{m'\nu}(\boldsymbol{k}',z_h) , \quad (19)$$

are the kinetic-energy and potential-energy terms, respectively.

Within the dipole approximation, the oscillator strength per unit area for the X state is defined as

$$f_X = \frac{2}{m_0 E_X} \left| \sum_\nu (\boldsymbol{\xi}\cdot\boldsymbol{P}^{\sigma\nu}_{cv}) \int dz\, \Psi^X_\nu(\boldsymbol{\rho}=0,z,z) \right|^2 = \frac{2}{m_0 E_X} \left| \sum_\nu (\boldsymbol{\xi}\cdot\boldsymbol{P}^{\sigma\nu}_{cv}) \sum_{n,m} \int \frac{d^2\boldsymbol{k}}{(2\pi)^2} \phi^X_{nm}(\boldsymbol{k})\, I^{\sigma\nu}_{nm}(\boldsymbol{k}) \right|^2 , \quad (20)$$

where

$$I^{\sigma\nu}_{nm}(\boldsymbol{k}) = \int dz\, f_{n\sigma}(\boldsymbol{k},z)\, g_{m\nu}(\boldsymbol{k},z) \quad (21)$$

is the overlap integral between the conduction and valence subbands, $\boldsymbol{\xi}$ is the polarization vector, and

$$\boldsymbol{P}^{\sigma\nu}_{cv} = \langle u^\sigma_c |\boldsymbol{p}| u^\nu_v \rangle \quad (22)$$

is the momentum matrix element between the conduction-band Bloch function,

$$u^{1/2}_c = |S\uparrow\rangle , \; u^{-1/2}_c = |S\downarrow\rangle , \quad (23)$$

and the valence-band Bloch function,

$$u^\nu_v = \left|\tfrac{3}{2},\nu\right\rangle , \; \nu = \tfrac{3}{2},\tfrac{1}{2},-\tfrac{1}{2},-\tfrac{3}{2} . \quad (24)$$

The polarization selection rules are embedded in the term $|\boldsymbol{\xi}\cdot\boldsymbol{P}^{\sigma\nu}_{cv}|^2$ of the oscillator strength formula (20), where u^ν_v can be further expressed as linear combinations of the wave function $|X\uparrow\rangle$, $|Y\uparrow\rangle$, $|Z\uparrow\rangle$, etc.[30,26] Because of the crystal symmetry properties, we have

$$\langle S|p_x|X\rangle = \langle S|p_y|Y\rangle = \langle S|p_z|Z\rangle = P_{cv} , \quad (25)$$

and all of the other terms such as $\langle S|p_x|Y\rangle$, $\langle S|p_x|Z\rangle$ are zeros. The resultant polarization selection rules for $|\boldsymbol{\xi}\cdot\boldsymbol{P}^{\sigma\nu}_{cv}|^2$ are summarized in Table I for the TE ($\boldsymbol{\xi}=\hat{\boldsymbol{x}}$ or $\hat{\boldsymbol{y}}$) and TM ($\boldsymbol{\xi}=\hat{\boldsymbol{z}}$) polarizations.

Finally, the absorption coefficient α at photon energy $\hbar\omega$ is calculated by summing up the contributions from all exciton states,

$$\alpha(\hbar\omega) = \left(\frac{\pi e^2\hbar}{n_r\epsilon_0 m_0 cL}\right) \sum_X \left(f_X \frac{\Gamma_X/\pi}{(\hbar\omega - E_X)^2 + {\Gamma_X}^2} \right) , \quad (26)$$

where c, L, and n_r are the speed of light in vacuum, the width of the quantum well, and the refraction index of the quantum-well material, respectively. In practice, the linewidth Γ_X due to various scattering mechanisms is chosen empirically to match the experimental data.

TABLE I. Polarization selection rules.

$\lvert\xi\cdot P^{\sigma\nu}_{cv}\rvert^2$	$\nu=3/2$	$\nu=1/2$	$\nu=-1/2$	$\nu=-3/2$
		TE polarization		
$\sigma=1/2$	$P^2_{cv}/2$	0	$P^2_{cv}/6$	0
$\sigma=-1/2$	0	$P^2_{cv}/6$	0	$P^2_{cv}/2$
		TM polarization		
$\sigma=1/2$	0	$2P^2_{cv}/3$	0	0
$\sigma=-1/2$	0	0	$2P^2_{cv}/3$	0

B. Angular-momentum quantum number

Since the exciton Hamiltonian (1) is not invariant under an arbitrary rotation around the z axis, it is not expected that the exciton state has a well-defined angular-momentum quantum number. To express explicitly the angular dependence, we expand the wave function, the kinetic-energy term, and the potential-energy term into a Fourier series

$$\phi^X_{nm}(k,\theta) = \sum_\ell \phi^{X\ell}_{nm}(k)\, e^{i\ell\theta} , \quad (27)$$

$$T_{nm}(k,\theta) = \sum_\ell T^\ell_{nm}(k)\, e^{i\ell\theta} , \quad (28)$$

$$V_{nmn'm'}(k,k',\theta,\theta') = \sum_\ell \sum_{\ell'} V^{\ell\ell'}_{nmn'm'}(k,k')\, e^{i\ell\theta} e^{-i\ell'\theta'} . \quad (29)$$

By multiplying Eq. (17) by $\exp(-i\nu\theta)$ and integrating it over θ from 0 to 2π, the exciton equation becomes

$$E_X\, \phi^{X\ell}_{nm}(k) = \sum_{\ell'} T^{\ell-\ell'}_{nm}(k)\, \phi^{X\ell'}_{nm}(k) + \sum_{n',m'} \sum_{\ell'} \int_0^\infty \frac{k'dk'}{2\pi} V^{\ell\ell'}_{nmn'm'}(k,k') \times \phi^{X\ell'}_{n'm'}(k') . \quad (30)$$

The above equation clearly shows that all of the different ℓ components of the wave function are coupled together, each of them having a nonzero contribution to the oscillator strength

$$f_X = \frac{2}{m_0 E_X}\left|\sum_\nu (\boldsymbol{\xi}\cdot\boldsymbol{P}_{cv}^{\sigma\nu})\sum_{n,m}\sum_\ell \int_0^\infty \frac{k\,dk}{2\pi}\int_0^{2\pi}\frac{d\theta}{2\pi}\,\phi_{nm}^X(k)\,I_{nm}^{\sigma\nu}(k,\theta)\,e^{i\ell\theta}\right|^2 . \tag{31}$$

Apparently, there does not exist a unique ℓ which can be assigned to the exciton state as an angular-momentum quantum number. Such an assignment becomes possible only if the axial approximation is made, that is, ignoring the warping of the valence-subband constant-energy surface in the quantum-well plane.

C. Axial approximation

This approximation gives very good results for the valence subband energies at small k_x and k_y with a finite k_z determined by the quantization energy in a quantum-well structure. The justifications of the axial approximation can be seen from the dispersion curves in Refs. 16–18, where the warping of the subband energies for the parallel $\boldsymbol{k}$ component less than about an inverse exciton radius is found to be negligible (less than a fraction of a meV for the lowest two bound valence subbands). Therefore, we would estimate that the warping of the valence subbands in the plane of the quantum well has an even smaller effect on the exciton binding energy[17] since the approximation appears in the off-diagonal terms of the Luttinger-Kohn Hamiltonian. The major consequences of the axial approximation[18,31,32,26] are (i) the valence-subband envelope functions have the form

$$g_{m\nu}(\boldsymbol{k},z_h) = g_{m\nu}(k,z_h)\,e^{-i\nu\theta}\ , \tag{32}$$

which takes into account the variations of the wave functions with the direction of $\boldsymbol{k}$ in the k_x-k_y plane, (ii) the valence-subband energy $E_m^h(\boldsymbol{k})$ becomes θ independent, as does the kinetic-energy term in the exciton equation

$$T_{nm}(k,\theta) = T_{nm}(k)\ , \tag{33}$$

and (iii) the potential-energy term depends only on the difference between θ and θ'

$$V_{nmn'm'}(k,k',\theta-\theta') = \sum_\ell V_{nmn'm'}^\ell(k,k')\,e^{i\ell(\theta-\theta')}\ , \tag{34}$$

where

$$V_{nmn'm'}^\ell(k,k') = -\frac{e^2}{2\epsilon_0\epsilon}\sum_\nu \int dz_e \int dz_h \int_0^{2\pi}\frac{d\theta}{2\pi}\,\frac{e^{-q\,|z_e-z_h|}}{q}\,e^{i(\sigma+\nu-\ell)\theta} f_n(k,z_e)\,f_{n'}(k',z_e)\,g_{m\nu}(k,z_h)\,g_{m'\nu}(k',z_h) \tag{35}$$

and

$$q = (k^2+k'^2-2kk'\cos\theta)^{1/2}\ . \tag{36}$$

As a result, different ℓ components in Eq. (30) become uncoupled and each of them satisfies a single-ℓ equation

$$T_{nm}(k)\phi_{nm}^{X\ell}(k) + \sum_{n',m'}\int_0^\infty \frac{k'dk'}{2\pi}\,V_{nmn'm'}^\ell(k,k')\,\phi_{n'm'}^{X\ell}(k') = E_{X\ell}\,\phi_{nm}^{X\ell}(k)\ . \tag{37}$$

In this case, ℓ becomes a well-defined angular-momentum quantum number and each exciton state can be labeled uniquely by an ℓ and X. Furthermore, the oscillator-strength formula is simplified to

$$f_{X\ell} = \frac{2}{m_0\hbar\omega}\left|\sum_\nu (\boldsymbol{\xi}\cdot\boldsymbol{P}_{cv}^{\sigma\nu})\sum_{n,m}\int_0^\infty \frac{k\,dk}{2\pi}\,\phi_{nm}^{X\ell}(k)\,I_{nm}^{\sigma\nu}(k)\,\delta_{\ell,\sigma+\nu}\right|^2 , \tag{38}$$

where

$$I_{nm}^{\sigma\nu}(k,\theta) = I_{nm}^{\sigma\nu}(k)\,e^{-i(\sigma+\nu)\theta} \tag{39}$$

and

$$I_{nm}^{\sigma\nu}(k) = \int dz\, f_{n\sigma}(k,z)\,g_{m\nu}(k,z)\ . \tag{40}$$

Now only four terms ($\ell=\sigma+\frac{3}{2}$, $\sigma+\frac{1}{2}$, $\sigma-\frac{1}{2}$, $\sigma-\frac{3}{2}$) have nonzero contributions, which means that the exciton equation (37) has to be solved at most four times. As discussed earlier, the conduction-band nonparabolicity effects are usually negligible, therefore, the k dependence of the electron wave function can be ignored, $f_{n\sigma}(k,z) = f_{n\sigma}(z)$. We also note that, after pulling out the θ dependence, the wave functions $f_{n\sigma}(z)$ and $g_{m\nu}(k,z_h)$ can be made real.

In the parabolic-band model for both the conduction and the valence bands, the exciton wave function is a one-component scalar and the states with $\ell=0$, ±1, ±2, and ±3 are traditionally called the s, p, d, and f states. Under the band-mixing model (with the axial approximation), the exciton wave function is a four-component spinor. Carrying out the θ integration in Eq. (15), we find that each component of the exciton wave function has a different angular dependence[16]

$$\Psi_{\nu}^{X\ell}(\boldsymbol{\rho}, z_e, z_h) = e^{i(\ell-\sigma-\nu)\theta} \sum_{n,m} \int_0^{\infty} \frac{kdk}{2\pi} \phi_{nm}^{X\ell}(k) f_{n\sigma}(k, z_e)\, g_{m\nu}(k, z_h) J_{\ell-\sigma-\nu}(k\rho) \ . \tag{41}$$

However, for each subband, there is usually one dominant component. For example, the hole spin index of the dominant component is equal to $\frac{3}{2}$ or $-\frac{3}{2}$ for heavy-hole subbands, and equal to $\frac{1}{2}$ or $-\frac{1}{2}$ for light-hole subbands. Therefore, we can still define the exciton to be an s, $p^{\pm}$, $d^{\pm}$, or $f^{\pm}$ state according to the angular dependence of the dominant component, that is, according to whether the value of $l-\sigma-\nu$ is 0, ±1, ±2, or ±3 for the dominant component.

III. RESULTS AND DISCUSSIONS

Even under the axial approximation, solving the integral equation (37) requires intensive computation. For instance, if two conduction subbands and two valence subbands are included and a 50-point Gaussian-quadrature method is used, the size of the final matrix equation to be solved is 400 × 400, taking into account the fact that, at $k \neq 0$, each valence subband is split into two subbands by the electric field. The equation has to be solved four times for four different angular-momentum quantum numbers and repeated 40 times for 40 electric fields. The most time-consuming part is the triple integral in Eq. (35) to calculate the Coulomb interaction term. In Sec. III A we adopt a simplified version of the model assuming s states exciton coupling only. The theoretical results are shown to compare well with the room-temperature experimental data of Miller, Weiner, and Chemla.[10] In Sec. III B numerical results using the full band-mixing model with axial approximation are compared with the low-temperature experimental data of Vina *et al.*[6] showing coupling of the exciton excited states.

A. Simplified model (s states only)

In this simplified model, the θ dependence of the envelope functions is neglected completely, that is, assuming

$$f_{n\sigma}(\boldsymbol{k}, z_e) = f_n(z_e) \ , \quad g_{m\nu}(\boldsymbol{k}, z_h) = g_{m\nu}(k, z_h) \ . \tag{42}$$

As a result, the Coulomb interaction term (35) and the oscillator strength formula (38) are simplified to [$q = (k^2 + k'^2 - 2kk'\cos\theta)^{1/2}$]

$$V_{nmn'm'}^{\ell=0}(k, k') = -\frac{e^2}{2\epsilon_0\epsilon} \sum_{\nu} \int dz_e \int dz_h \int_0^{2\pi} \frac{d\theta}{2\pi} \frac{e^{-q\,|z_e - z_h|}}{q} f_n(z_e)\, f_{n'}(z_e)\, g_{m\nu}(k, z_h)\, g_{m'\nu}(k', z_h) \ , \tag{43}$$

and

$$f_{X\ell} = \frac{2}{m_0 E_X} \left| \sum_{\nu} (\boldsymbol{\xi} \cdot \boldsymbol{P}_{cv}^{\sigma\nu}) \sum_{n,m} \int_0^{\infty} \frac{kdk}{2\pi} \phi_{nm}^{X\ell}(k)\, I_{nm}^{\sigma\nu}(k)\, \delta_{\ell,0} \right|^2 \ , \tag{44}$$

respectively. Under this model, according to Eq. (43), only the s state ($\ell = 0$) is optically active. Therefore, the computational time is cut down to about one-quarter of that required by the original model, but still takes about 2.5 min in the Cray Y-MP supercomputer. This was the exciton theory with valence-band mixing before Zhu and Huang[16] pointed out the significance of the angular dependence of the exciton. The adoption of this simplified model is encouraged by the early work of Sanders and Chang,[33] who ignored the θ-dependence and were able to explain the experimental data.

Figures 1(a) and 1(b) show the room-temperature absorption spectra at various electric fields for the TE and TM polarizations measured by Miller, Weiner, and Chemla.[10] The sample was a GaAs/$Al_{0.3}Ga_{0.7}As$ double-well structure with 94-Å-wide wells. The zero-field spectra clearly exhibit the polarization selection rules summarized in Table I. For the TE polarization, both the heavy-hole and the light-hole excitons appear. For the TM polarization, the heavy-hole exciton disappears and the light-hole exciton increases in strength.

When a perpendicular electric field is applied, a large shift of the absorption edge to lower energy is seen in both polarizations as a result of the quantum-confined Stark effect.[9] The maximum shift observed in the experiment was 40 meV for the light-hole exciton with the TM polarization at a field of 220 kV/cm.[10] This is ten times the bulk exciton binding energy and occurs at an applied field 100 times that of the classical exciton ionization field. Even larger relative shifts have recently been seen in single-well luminescence experiments at low temperature.[34] It is remarkable that at such high fields, the exciton resonances are still clearly resolvable, with very little broadening.

Theoretically calculated absorption spectra are shown in Figs. 2(a) and 2(b), and the experimental and calculated exciton peaks are compared in Fig. 3, which demonstrate an excellent agreement between theory and experiments.

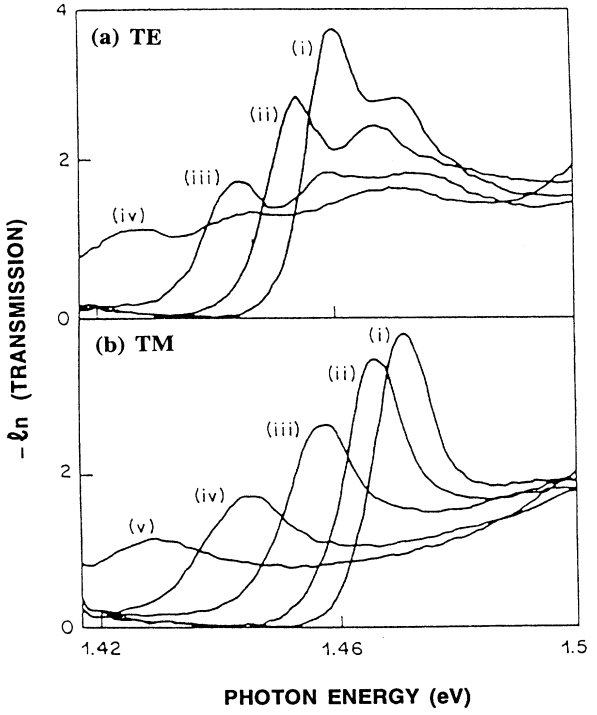

FIG. 1. Absorption spectra of a GaAs/$Al_{0.3}Ga_{0.7}As$ quantum-well waveguide as a function of field: (i) 0 kV/cm, (ii) 60 kV/cm, (iii) 100 kV/cm, (iv) 150 kV/cm, (v) 200 kV/cm. (a) TE polarization, (b) TM polarization. [After Miller, Weiner, and Chemla (Ref. 10).]

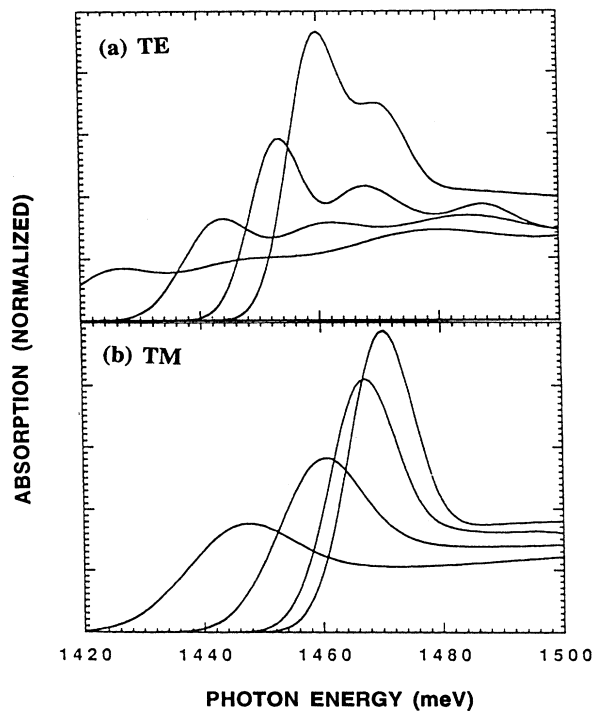

FIG. 2. Theoretically calculated absorption spectra for the quantum-well waveguide. (a) TE polarization, (b) TM polarization.

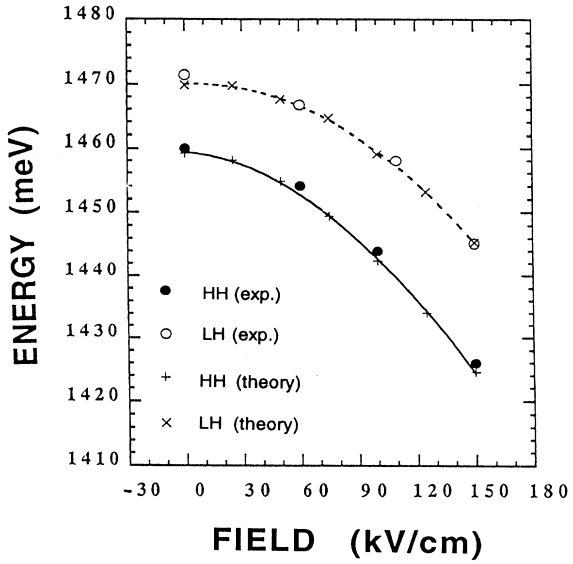

FIG. 3. Comparison of experimental and theoretically calculated exciton energies vs electric fields.

B. Full band-mixing model with axial approximation

The evidence of the heavy-hole and light-hole exciton mixings observed by Viña *et al.*[6] and the interpretation of their experimental data are discussed in this section.

The sample used by Viña *et al.*[6] was a GaAs/$Al_xGa_{1-x}As$ *p-i-n* heterostructure grown by molecular-beam epitaxy. The intrinsic region is about 3.5-μm wide and consists of a series of five 160-Å-wide GaAs quantum wells with 250-Å-wide $Al_{0.35}Ga_{0.65}As$ barriers, capped between two 800-Å-thick $Al_{0.35}Ga_{0.65}As$ buffer layers. The electric field perpendicular to the quantum-well layers is applied by biasing of the structure between the p^+ and n^+ GaAs regions. The magnitude of the electric field, estimated from growth parameters and from the bias corresponding to the flat band condition (1.7–1.75 V), is believed to be accurate within 10%. Excitation spectra were recorded at 4.8 K with a resolution of 0.2 meV.

To begin with, we plot in Fig. 4 the band-edge transition energies (solid curves) as a function of electric fields for the quantum-well structures described above and the exciton transition energies (dashed lines) calculated by ignoring the coupling between the heavy-hole (HH) and light-hole (LH) subbands and the angular dependence of the envelop functions (i.e., assuming a simple two-band model). If the assumption were true, we would expect that only the *s*-state excitons were optically active and that the HH-2*s* state would cross over with the LH-1*s* state at an electric field around 12 kV/cm.

However, experimental data contain much more details. The PLE spectra of Viña *et al.*[6] for several bias voltages are shown in Fig. 5(a). Two pronounced peaks, attributed to the ground state of the C1-LH1 exciton and the excited state of the C1-HH1 exciton, are labeled ℓ_1 and $h_1^{(2x)}$, $2x$ meaning the excited state $2s$ and $2p$.

First, we observe that in a certain field range (8–

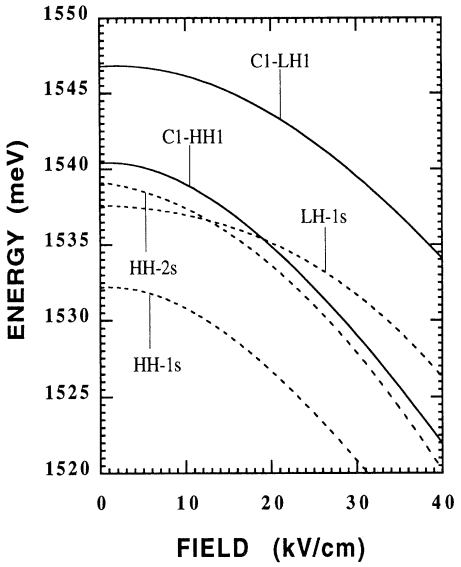

FIG. 4. Band-edge transition energies (solid curves) vs electric fields and the exciton energies (dashed curves) calculated by ignoring the coupling between the heavy-hole and light-hole subbands and the angular dependence of the envelop functions.

16 kV/cm), a repulsion between the HH-2x and the LH-1s exciton peaks becomes noticeable in Fig. 5(a); it is more clearly shown in Fig. 6(a), where the energies of the two excitons are plotted versus the electric field. Second, in a finer scale, the PLE spectra in Fig. 7(a) reveal that the exciton peak 2x in Fig. 5(a) actually consists of two peaks, labeled 2s and 2p in Fig. 7(a).

The theoretically calculated exciton energies and absorption spectra are shown in Figs. 5(b), 6(b), and 7(b) and are compared to the original experimental data. Although the absorption spectra and the photoluminescence spectra are different in nature, they can still be compared qualitatively. The calculation was based on the theory presented in Sec. II, with the material parameters taken from Ref. 35 For the Luttinger parameters, we chose γ_1=6.80, γ_2=1.90, γ_3=2.73 for GaAs, and γ_1=3.45, γ_2=0.68, γ_3=2.19 for AlAs. A linear interpolation is used for the parameters in $Al_xGa_{1-x}As$ barrier regions.

For convenience, the field axis (x axis) in Fig. 6 is roughly divided into three intervals: from 0 to 8 kV/cm, from 8 to 16 kV/cm, and from 16 to 50 kV/cm, which are referred to as the low-field regime, the strong-coupling regime, and the high-field regime, respectively.

In the low-field regime, the HH-2x exciton has an energy 1.5-meV higher than that of the LH-1s exciton, but the LH-1s exciton has an oscillator strength three to four times larger than that of the HH-2x exciton. The Stark shifts for both the HH-2x exciton and the LH-1s exciton are less than 0.2 meV. The strong-coupling regime is where the anticrossing takes place. The calculated oscillator strengths of the LH and HH exciton states are shown in Fig. 8.

Figures 7 and 8 show that, at zero field, the 2p excited state has a negligible oscillator strength. With increasing field, the 2p state appears as a shoulder on the lower-energy side of the spectra and becomes comparable in amplitude to the 2s state near F = 9.5 kV/cm. When the field continues to increase, the 2s state disappears quickly as a result of field ionization and the 2p state eventually

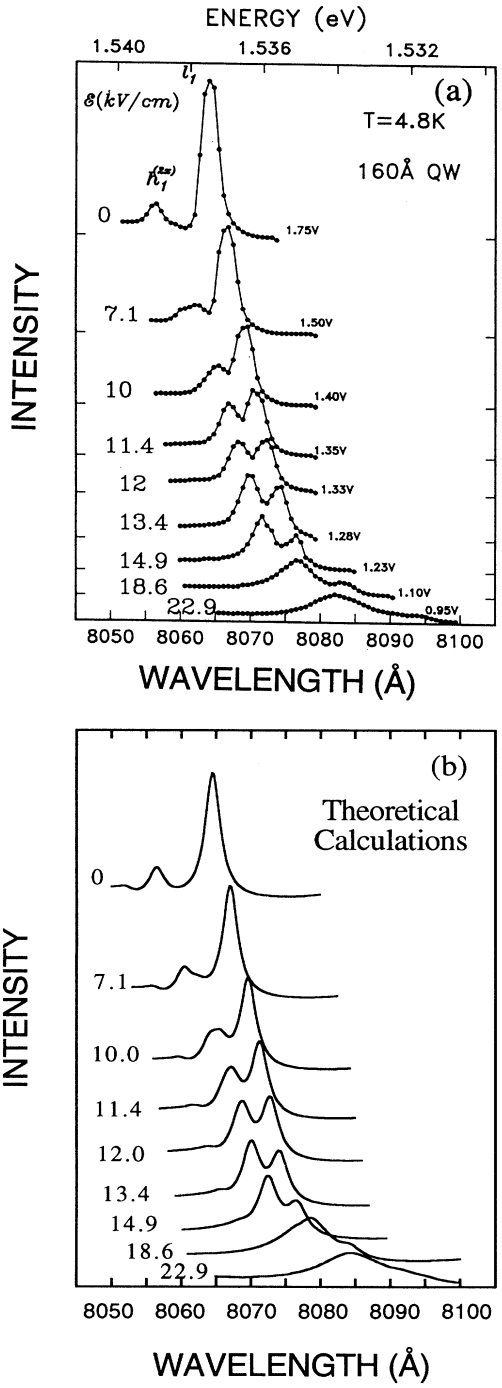

FIG. 5. (a) Photoluminescence excitation spectra measured on an $Al_{0.35}Ga_{0.65}As$ multiple-quantum-well structure with 160-Å-wide wells for several bias voltages [after Viña *et al.* (Ref. 6)]. (b) Calculated exciton absorption spectra at several electric fields, which can be qualitatively compared with the photoluminescence excitation spectra in (a).

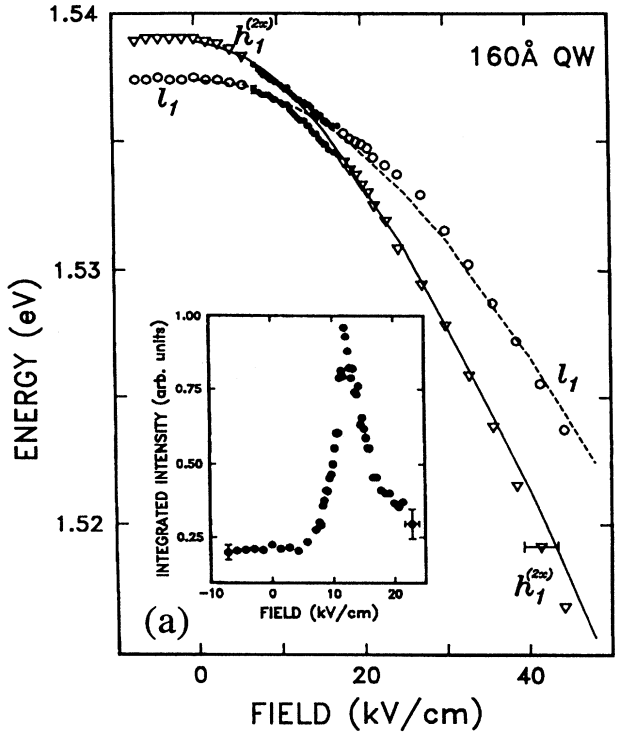

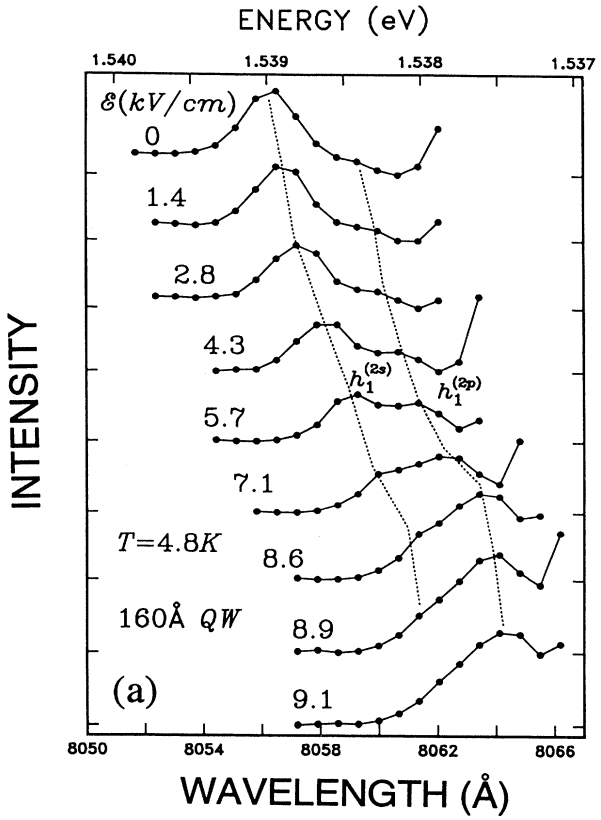

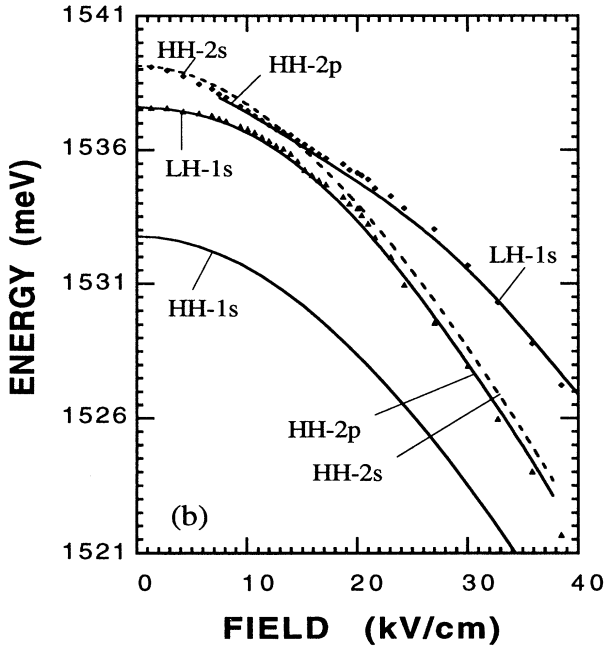

FIG. 6. (a) Energies of the ground state of the light-hole exciton (l_1) and the excited state of the heavy-hole exciton ($h_1^{(2s)}$) as functions of electric field. Inset: The integrated intensity of the $h_1^{(2s)}$ peak normalized to that of the l_1 peak as a function of field [after Viña *et al.* (Ref. 6)]. (b) Theoretically calculated exciton energies (solid and dashed curves) using the full band-mixing model compared with the experimental data (solid triangles and diamonds).

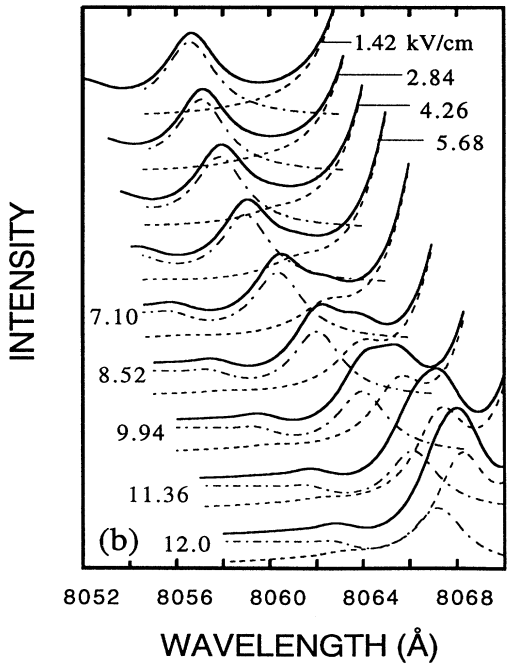

FIG. 7. (a) Photoluminescence excitation spectra measured on an $Al_{0.35}Ga_{0.65}As$ multiple-quantum-well structure with 160-Å-wide wells for small bias fields [after Viña *et al.* (Ref. 6)]. (b) Calculated exciton absorption spectra at small electric fields, which can be qualitatively compared with the photoluminescence excitation spectra in (a).

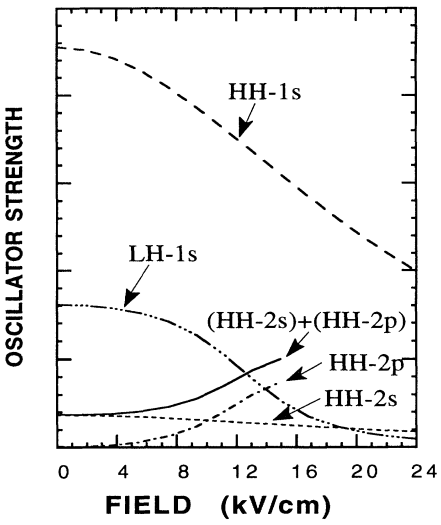

FIG. 8. The oscillator strengths of HH-1s, HH-2s, HH-2p, LH-1s, and the sum of HH-2s and HH-2p as functions of the electric field.

becomes dominant at higher fields. The energy difference between the 2s and the 2p states is roughly 0.5 meV. Apparently, in the strong-coupling regime, it is the 2p state, rather than the 2s state, of the heavy-hole exciton that couples strongly with the 1s state of the light-hole exciton. This conclusion agrees with the recent study of Wen and Chang;[36] however, their results did not resolve the 2s and 2p states.

Theoretically, it can be understood why the LH-1s state couples with the HH-2p state, not with the HH-2s state. Recall that the s and p states are defined as $\ell-\sigma-\nu=0$ and $\ell-\sigma-\nu=\pm1$, respectively, for the dominant components of the exciton spinors. Also remember that the dominant component of the hole wave function has $\nu=\pm\frac{3}{2}$ for heavy holes and $\nu=\pm\frac{1}{2}$ for light holes. Therefore, the exciton states have the following characteristics: for HH-2s,

$$(\ell=1,\sigma=-\tfrac{1}{2},\nu=\tfrac{3}{2}) \text{ or } (\ell=-1,\sigma=\tfrac{1}{2},\nu=-\tfrac{3}{2}) ,$$

for HH-2p,

$$(\ell=0,\sigma=\tfrac{1}{2},\nu=-\tfrac{3}{2}) \text{ or } (\ell=0,\sigma=-\tfrac{1}{2},\nu=\tfrac{3}{2}) ,$$

and for LH-1s,

$$(\ell=0,\sigma=\tfrac{1}{2},\nu=-\tfrac{1}{2}) \text{ or } (\ell=0,\sigma=-\tfrac{1}{2},\nu=\tfrac{1}{2}) . \tag{45}$$

Since different ℓ components in the exciton equation are decoupled under the axial approximation [see Eq. (37)], it becomes clear that the LH-1s state ($\ell=0$) should couple with the HH-2p state ($\ell=0$), but not with the HH-2s state ($\ell=\pm1$).

The HH-2x exciton and LH-1s exciton move closer to each other in energy as the electric field increases from 8 to 12 kV/cm. At the same time, as shown in Figs. 6, 7, and 8, the HH-2p exciton begins to pick up oscillator strength while the LH-1s exciton loses oscillator strength steadily, indicating a strong coupling between them. The energy separation between these two excitons reaches a minimum of 0.64 meV at 12 kV/cm (resonant field). At this point, the two excitons almost have equal oscillator strength and the coupling reaches its maximum. As the field increases farther into the high-field regime, the HH-2p exciton and the LH-1s exciton become uncoupled again. The HH-2p exciton is shifted to the lower-energy side much faster than the LH-1s exciton.

In summary, the theory is able to predict the most important anticrossing behavior at the correct resonant field (12 kV/cm) with the correct minimum energy split (6.4 meV). The fine structures of the 2s and 2p exciton states are also accounted for in our results. The calculation is done without any adjustable parameters except that the linewidths at various fields are chosen empirically to account for the field-broadening effects. The experimental estimated field has an uncertainty of $\pm10\%$. Within such an uncertainty, we are able to scale the electric field and match the data perfectly.

IV. CONCLUSIONS

The mixing of the valence subbands of semiconductor quantum wells has been the topic of much theoretical and experimental work. At the zone center the heavy- and light-hole subbands exactly decouple from each other, but this is not the case for finite k. For $k\neq0$, the heavy- and light-hole bands are highly intermixed, leading to a strongly nonparabolic subband structure.

There are several important consequences of the heavy- and light-hole intermixings away from the zone center; for instance, resonant tunneling between the heavy hole and the light hole becomes possible; polarization selection rules break down;[37] and hole tunneling times are more rapid.[38]

The experimental observation by Vinã has provided one of the most direct evidences of heavy-hole and light-hole mixings. In this paper a complete exciton theory based on the band-mixing model is presented and used to interpret the data. The excellent agreement between the theoretical calculation and the experimental data has demonstrated that the current theory can be used reliably to model realistic devices, such as the electroabsorption modulators and self-electro-optic effect devices (SEED's).

ACKNOWLEDGMENTS

We thank Professor Y. C. Chang for helpful discussions. This work was supported by the U.S. Office of Naval Research (Grant No. N00014-90-J-1821). The computation time was provided by the National Center for Supercomputer Applications at the University of Illinois, Urbana-Champaign.

APPENDIX: NUMERICAL SOLUTIONS IN MOMENTUM SPACE

In this appendix we present our theoretical method for solving the effective-mass equation for exciton mixing in

momentum space. Typically, the integral equation (37) has to be solved for four ℓ values. For example, if $\sigma = \frac{1}{2}$, we find $\ell = 2, 1, 0, -1$. There are four independent equations in Eq. (37) assigned by each ℓ to be solved in $\boldsymbol{k}$ space. Numerically, we find the solutions for the last two ℓ values (0 and -1) are the same as those for the first two ($\ell = 1$ and 2). The solution technique is similar to the approach in Ref. 23 . Here we summarize the major steps and a few important analytical expressions. The major steps are to take care of the singularity in the Coulomb potential in the integral of Eq. (37). Let us write the integral as

$$
\begin{aligned}
I(k_i) &= \int_0^\infty \frac{k'dk'}{2\pi} V^{\ell}_{nmn'm'}(k_i,k')\phi^{X\ell}_{n'm'}(k') \\
&= \sum_{j\neq i}^{N} \frac{k_j}{2\pi}\left(\frac{dk}{dx}\right)_j w_j V^{\ell}_{nmn'm'}(k_i,k_j)\phi^{X\ell}_{n'm'}(k_j) + \frac{k_i}{2\pi}\left(\frac{dk}{dx}\right)_i w_i \left[V^{\ell}_{nmn'm'}(k_i,k_i) - \mathcal{V}^{\ell}_{nmn'm'}(k_i,k_i)\right]\phi^{X\ell}_{n'm'}(k_i) \\
&\quad - \left[\sum_{j\neq i}^{N} \frac{k_j}{2\pi}\left(\frac{dk}{dx}\right)_j w_j \mathcal{V}^{\ell}_{nmn'm'}(k_i,k_j)\right]\phi^{X\ell}_{n'm'}(k_i) + \left[\int_0^\infty \frac{k'dk'}{2\pi}\mathcal{V}^{\ell}_{nmn'm'}(k_i,k')\right]\phi^{X\ell}_{n'm'}(k_i) \,, \qquad \text{(A1)}
\end{aligned}
$$

where we have written the original integral in terms of the Gaussian quadrature summation formula. We have added the last term containing the integral $\mathcal{V}^{\ell}_{nmn'm'}$ and subtracted it again. The diagonal terms for $k_i = k_j$ have been written out explicitly to be calculated in the following. Here $k = k_0 \tan\left(\frac{\pi}{2}x\right)$, $k_0 (= 0.01/\text{Å})$ is a constant and $0 < x < 1$. N is the number of quadrature points and x_i and w_i are the roots and weighting functions in the quadrature formula. We introduce

$$
\begin{aligned}
\mathcal{V}^{\ell}_{nmn'm'}(k,k') &\equiv \frac{2k^2}{k^2+k'^2}\left(\frac{-e^2}{2\epsilon_0\epsilon}\right)\sum_\nu \int dz_e \int dz_h f_n(z_e) f_{n'}(z_e) g_{m\nu}(k,z_h) g_{m'\nu}(k,z_h) \int_0^{2\pi} \frac{d\varphi}{2\pi}\frac{1}{q}\cos(\mu\varphi) \\
&= \frac{2k^2}{k^2+k'^2}\delta_{nn'}\delta_{mm'}\int_0^{2\pi}\frac{d\varphi}{2\pi}\left(\frac{-e^2}{2\epsilon_0\epsilon q}\right)\cos(\mu\varphi) \,, \qquad \text{(A2)}
\end{aligned}
$$

where $\mu = \sigma + \nu - i$ and q is given in Eq. (36). A weighting function of the form $2k^2/(k^2+k'^2)$ is added for improving numerical convergence.

The first term in Eq. (A1) requires $k_i \neq k_j$. Therefore, $k \neq k'$.

$$
V^{\ell}_{nmn'm'}(k,k') = \frac{e^2}{8\pi\epsilon\epsilon_0}\int dz_e \int dz_h \sum_\nu U^{\mu=\sigma+\nu-\ell}(k,k',|z_e-z_h|) f_n(z_e) f_{n'}(z_e) g_{m\nu}(k,z_h) g_{m'\nu}(k',z_h) \,, \qquad \text{(A3)}
$$

where

$$
U^{\mu}(k,k',Z) = -4\pi\int_0^{2\pi}\frac{d\varphi}{2\pi}\frac{e^{-qZ}}{q}\cos(\mu\varphi) = \frac{-4}{\sqrt{kk'}}\mathcal{U}^{\mu}(D,X) \,, \qquad \text{(A4)}
$$

$$
\mathcal{U}^{\mu}(D,X) = \int_0^{\frac{\pi}{2}} d\theta \frac{\cos(2\mu\theta)}{\sqrt{D^2+\sin^2\theta}} e^{-X\sqrt{D^2+\sin^2\theta}} \,, \qquad \text{(A5)}
$$

$$
D \equiv \frac{|k-k'|}{2\sqrt{kk'}} \,, \qquad \text{(A6)}
$$

and

$$
X = 2\sqrt{kk'}Z \,. \qquad \text{(A7)}
$$

The large square brackets in the second term of Eq. (A1) can be written as

$$
\begin{aligned}
\left[V^{\ell}_{nmn'm'}(k,k) - \mathcal{V}^{\ell}_{nmn'm'}(k,k)\right] &= \frac{e^2}{8\pi\epsilon_0\epsilon}\int dz_e \int dz_h \sum_\nu 4\pi|z_e-z_h| G^{\mu}(k|z_e-z_h|) \\
&\quad \times f_n(z_e) f_{n'}(z_e) g_{m\nu}(k,z_h) g_{m'\nu}(k,z_h) \,, \qquad \text{(A8)}
\end{aligned}
$$

where

$$
G^{\mu}(k|z_e-z_h|) = \int_0^{2\pi}\frac{d\varphi}{2\pi}\frac{(1-e^{-2k|z_e-z_h|\sin\frac{\varphi}{2}})}{2k|z_e-z_h|\sin\frac{\varphi}{2}}\cos(\mu\varphi) \,. \qquad \text{(A9)}
$$

In the third term of Eq. (A1), we have ($k \neq k'$),

$$\mathcal{V}^{\ell}_{nmn'm'}(k,k') = \delta_{nn'}\delta_{mm'}\frac{2k^2}{k^2+k'^2}\left(\frac{e^2}{8\pi\epsilon_0\epsilon}\right)V^{\mu}(k,k') \ , \tag{A10}$$

where

$$V^{\mu}(k,k') = -4\pi\int_0^{2\pi}\frac{d\varphi}{2\pi}\frac{\cos\mu\varphi}{\sqrt{k^2+k'^2-2kk'\cos\varphi}}$$
$$= \frac{-4}{\sqrt{kk'}}\sinh^{-1}\left(\frac{\pi}{2D}\right)\int_0^1\cos(2\mu\theta)\frac{D\cosh\alpha}{\sqrt{D^2+\sin^2\theta}}dt \ , \tag{A11}$$

$$\alpha = t\sinh^{-1}\left(\frac{\pi}{2D}\right) \ , \tag{A12}$$

and

$$\theta = D\sinh\alpha \ . \tag{A13}$$

The last term in Eq. (A1) can be integrated numerically using the function $V^{\mu}(k,k')$ to have the form

$$\int_0^{\infty}\frac{k'dk'}{2\pi}\mathcal{V}^{\ell}_{nmn'm'}(k,k') = \left(\frac{e^2}{8\pi\epsilon_0\epsilon}\right)\delta_{nn'}\delta_{mm'}(-C_{\mu}k) \ , \tag{A14}$$

where

$C_0 = 5.2442$,
$C_1 = 1.6037$,
$C_2 = 0.918\,63$,

and

$$C_3 = 0.637\,77. \tag{A15}$$

It should be pointed out that in the numerical approach, it is computationally convenient to tabulate the functions U^{μ}, G^{μ}, V^{μ}, etc. in terms of discrete k_i and $|z| = |z_e - z_h|$. Since $\mu = \sigma + \nu - \ell$, and $\cos(\mu\varphi) = \cos(-\mu\varphi)$, we need only $\mu = 0, 1, 2$, and 3. For $0 \leq z_e \leq L$, where L is the total width of the quantum well and the barriers, we only need $0 \leq |z_e - z_h| \leq L$.

*Present Address: Technology Product Division, IBM Corporation, Essex Junction, VT 05452.

[1]G. Bastard, *Wave Mechanics Applied to Semiconductor Heterostructures* (Wiley, New York, 1988).
[2]C. Weisbuch and B. Vinter, *Quantum Semiconductor Structures* (Academic, San Diego, 1991).
[3]*Semiconductors and Semimetals*, edited by R. K. Willardson and A. C. Beer (Academic, New York, 1987), Vol. 24.
[4]R. C. Miller, A. C. Gossard, G. D. Sanders, Y. C. Chang, and J. N. Schulman, Phys. Rev. B **32**, 8452 (1985).
[5]L. W. Molenkamp, G. E. W. Bauer, R. Eppenga, and C. T. Foxon, Phys. Rev. B **38**, 6147 (1988).
[6]L. Viña, R. T. Collins, E. E. Mendez, and W. I. Wang, Phys. Rev. Lett. **58**, 832 (1987); **59**, 602 (1987).
[7]J. M. Luttinger and W. Kohn, Phys. Rev. **97**, 869 (1955).
[8]J. M. Luttinger, Phys. Rev. **102**, 1030 (1956).
[9]D. A. B. Miller, D. S. Chemla, T. C. Damen, A. C. Gossard, W. Wiegmann, T. H. Wood, and C. A. Burrus, Phys. Rev. B **32**, 1043 (1985).
[10]D. A. B. Miller, J. S. Weiner, and D. S. Chemla, IEEE J. Quantum Electron. **QE-22**, 1816 (1986).
[11]P. Dawson, K. J. Moore, G. Duggan, H. I. Ralph, and C. T. Foxon, Phys. Rev. B **34**, 6007 (1986).
[12]K. J. Moore, P. Dawson, and C. T. Foxon, Phys. Rev. B **34**, 6022 (1986).
[13]E. S. Koteles and J. Y. Chi, Phys. Rev. B **37**, 6332 (1988).
[14]D. C. Reynolds, K. K. Bajaj, C. Leak, G. Peters, W. Theis, P. Yu, K. Alavi, C. Colvard, and I. Shidlovsky, Phys. Rev. B **37**, 3117 (1988).
[15]W. M. Theis, G. D. Sanders, C. E. Leak, D. C. Reynolds, Y. C. Chang, K. Alavi, C. Colvard, and I. Shidlovsky, Phys. Rev. B **39**, 1442 (1989).
[16]B. Zhu and K. Huang, Phys. Rev. B **36**, 8102 (1987); B. Zhu, *ibid.* **37**, 4689 (1987).
[17]G. E. W. Bauer and T. Ando, Phys. Rev. B **38**, 6015 (1988).
[18]L. C. Andreani and A. Pasquarello, Phys. Rev. B **42**, 8928 (1990); L. C. Andreani, A. Pasquarello, and F. Bassani, *ibid.* **36**, 5887 (1987).
[19]H. Chu and Y. C. Chang, Phys. Rev. B **39**, 10 861 (1989).
[20]D. A. Broido, E. S. Koteles, C. Jagannath, and J. Y. Chi, Phys. Rev. B **37**, 2725 (1988); D. A. Broido and S.-R. E. Yang, *ibid.* **42**, 11 051 (1990).
[21]J. P. Loehr and J. Singh, Phys. Rev. B **41**, 3695 (1990); **42**, 7154 (1990).
[22]R. Ataanasov and F. Bassani, Solid State Commun. **84**, 71 (1992).
[23]S. L. Chuang, S. Schmitt-Rink, D. S. Chemla, and D. A. B. Miller, Phys. Rev. B **43**, 1500 (1991).
[24]A. M. Fox, D. A. B. Miller, J. E. Cunningham, W. Y. Jan, C. Y.-P. Chao, and S. L. Chuang, Phys. Rev. B **46**, 15 365 (1992).
[25]C. Y.-P. Chao and S. L. Chuang, Phys. Rev. B **43**, 6530 (1991).
[26]C. Y.-P. Chao and S. L. Chuang, Phys. Rev. B **46**, 4110 (1992).
[27]E. O. Kane, J. Phys. Chem. Solids **1**, 82 (1956).
[28]E. O. Kane, J. Phys. Chem. Solids **1**, 249 (1957).
[29]E. O. Kane, in *Semiconductors and Semimetals*, edited by

R. K. Willardson and A. C. Beer (Academic, New York, 1966), Vol. 1, p. 75.
[30]D. Ahn and S. L. Chuang, IEEE J. Quantum Electron. **QE-24**, 2400 (1988); S. L. Chuang, Phys. Rev. B **43**, 9649 (1991).
[31]D. A. Broido and L. J. Sham, Phys. Rev. B **31**, 888 (1985).
[32]A. T. Twardowski and C. Herman, Phys. Rev. B **35**, 8144 (1987).
[33]G. D. Sanders and Y. C. Chang, Phys. Rev. B **35**, 1300 (1987).
[34]H. J. Polland, L. Schultheis, J. Kuhl, E. O. Gobel, and C. W. Tu, Phys. Rev. Lett. **55**, 2610 (1985).
[35]*Numerical Data and Functional Relationships in Science and Technology*, edited by K.-H. Hellwege, Landolt-Börnstein, New Series, Group III, Vol. 17a (Springer, Berlin, 1982); Groups III-V, Vol. 22a (Springer, Berlin, 1986).
[36]G. Wen and Y. C. Chang, Phys. Rev. B **45**, 6101 (1992).
[37]J. S. Weiner, D. S. Chemla, D. A. B. Miller, H. A. Haus, A. C. Gossard, W. Wiegmann, and C. A. Burrus, Appl. Phys. Lett. **47**, 664 (1985).
[38]E. T. Yu, M. K. Jackson, and T. C. McGill, Appl. Phys. Lett. **55**, 744 (1989).